Appendix A. Supplementary data

For: **Cathodoluminescence of iron oxides and oxyhydroxides**

By: Nir Galili, Ifat Kaplan-Ashiri and Itay Halevy.

Fe oxide and oxyhydroxide synthesis

Goethite was synthesized by three different methods. Synthetic goethite 1 (SynG1) was prepared by the method of Galili et al. (2019). First, 2-line ferrihydrite was prepared by dissolving 40 grams of $Fe(NO_3)_3 \cdot 9H_2O$ in 500 ml of doubly distilled water (DDW, 18.2 MΩ cm) and adjusting the pH of the solution to 7 by adding a 1 mol/L NaOH solution (Schwertmann and Cornell, 1991). The solution was vigorously stirred, and the fresh precipitates underwent a series of rinsing and washing cycles using deoxygenated DDW (by purging with 99.99% N_2). Finally, a suspension of the precipitates was purged with N_2 gas for 1 hour to remove any O_2 present in solution. The deaerated suspension was transferred to an anaerobic glovebox (O_2<1 ppm), where 10 ml aliquots of ferrihydrite suspension were transferred into a glass bottle. Buffered solutions of 0.05 mol/L total Fe(II) were prepared by dissolving $Fe(NH_4)_2(SO_4)_2 \times 6H_2O$ in a deoxygenated 0.1 mol/L 4-(2-hydroxyethyl)-1-piperazineethanesulfonic acid (HEPES) buffer and titrating to pH 7 using purged 0.5 M NaOH. 5 ml of the buffered solution were introduced into the glass bottle with the ferrihydrite (the ratio of Fe(II) to total Fe was ≈0.45). The bottles were then vigorously stirred, sealed with butyl rubber stoppers, crimped and quickly brought to their designated aging temperatures (60°C). The precipitates aged for 1 day, after which they were separated from the solution and dried, as described in the main text.

Synthetic goethite 2 (SynG2) was prepared from an alkaline solution, following the method described in Schwertmann & Cornell (1991). Briefly, 1 mol/L $Fe(NO_3)_3$ solution was mixed with 5 mol/L NaOH solution in a polyethylene flask and heated to 70°C. The suspension's initial pH

was ≈13.6. The precipitates aged at 70°C for 3 days, after which they were separated from the solution and dried, as described in the main text.

Synthetic goethite 3 (SynG3) was prepared as the Mn-free endmember of a series of Mn-substituted goethites. Ferrihydrite was precipitated by adding a 1 mol/L NaOH solution to solutions of $FeCl_3 \times 6H_2O$ and $MnCl_2 \times 4H_2O$ with Mn/(Mn + Fe) mole ratios between 0 and 28.5 %. The pH of the suspensions ranged from 11 to 11.5. The suspensions were left to age at a temperature of 90°C for 7 days, after which they were separated from the solution and dried, as described below. The exact Mn mole ratios were determined by ICP-MS analyses of the goethite, pre-treated with a 1 mol/L $MgCl_2$ solution to remove any exchangeable ions (Poulton and Canfield, 2005). A selected subset of these goethite samples, with 0, 1.4, 7.7, 15.5 and 24.6 mole % Mn, were examined by XRD and SEM.

Hematite was also synthesized by three different methods. Synthetic hematite 1 (SynH1) was prepared by the method of Galili et al. (2019). Doubly distilled water (18.2 MΩ cm), 1 mol/L NaOH and 1 mol/L $NaHCO_3$ solutions were prepared and purged with N_2 gas (99.99%) for 2 hours to remove dissolved O_2. The bottles were then sealed and transferred to an anaerobic glovebox (O_2<1 ppm). Inside the glovebox, 3.35 grams of reagent-grade $FeCl_3 \times 6H_2O$ were added to 63 ml of DDW in a glass bottle. Subsequently, ferrihydrite precipitated upon the addition of 37.5 ml of 1 mol/L NaOH, and the suspensions were stirred to avoid formation of aggregates. Then, 8.5 ml of 1 mol/L $NaHCO_3$ were added to the glass bottles, which were then sealed with butyl rubber stoppers, crimped and vigorously shaken. All solutions were heated on a hot plate to the designated aging temperature (60°C) before mixing. Sealed solutions were left to age for 30 days, after which the solids were separated from the solutions and dried, as described in the main text.

Synthetic hematite 2 (SynH2) was prepared by adding $FeCl_3 \times 6H_2O$ to a 0.002 M HCl solution, aged at 95°C in an oven for a week, following Schwertmann & Cornell (1991). The suspension's initial pH was ≈2. After aging, the solids were separated from the solutions and dried, as described in the main text.

Synthetic hematite 3 (SynH3) was prepared as the Mn-free endmember of a series of Mn-substituted hematites, which were formed by heating aliquots of some of the Mn-substituted goethite samples described above (with 0, 1.4, 7.7, 15.5, 28.5 mole % Mn) at 500°C for 24 hours. These samples were analyzed by XRD and SEM (Figs. A1 and A2) and confirmed to be pure hematite.

Magnetite was synthesized in two different ways. Synthetic magnetite 1 (SynM1) was prepared by mixing 65 mmol/L $FeCl_2 \times 4H_2O$ and 65 mM $FeCl_3 \times 6H_2O$ stock solutions in an artificial seawater solution and aging at 70°C for 6 months. The entire synthesis was done in an anaerobic chamber. Artificial seawater was prepared according to Table A2. The water was purged for 3 hours with N_2 gas to remove O_2. All salts, except $NaHCO_3$ were added prior to purging. After purging, the bottles were sealed with large butyl rubber stoppers until transferred to the glovebox, where the iron-rich stock solutions were added. Both the total Fe(II) and total Fe(III) concentrations were set to 1 mM, and the initial pH was adjusted to 7.5 by titration of a 1 M NaOH solution. After Fe addition, the bottles were sealed again with butyl rubber stoppers, crimped and vigorously shaken, and moved to an oven set to 70°C. After aging, the solids were separated from the solutions and dried, as described in the main text. In addition to the magnetite synthesized in this study, we examined a commercially available magnetite (SynM2, Sigma Aldrich).

Natural sample screening and preparation

The natural samples analyzed in this study are listed in Table A1. Prior to analysis by SEM-CL, natural samples were screened to verify that they contained the minerals of interest. This screening involved mineral purification protocols (Galili et al., 2019), after which the minerals of interest were identified in all natural samples. In addition to the minerals of interest, the natural goethite samples NatG1 and NatG3 contained poorly crystalline Fe hydroxides and silica, and the natural hematite samples NatH1, NatH2 and NatH3 contained minor amounts of quartz and possibly other silicate minerals (Fig. A1). The SEM-CL spectra were collected from regions a few microns in diameter, which contained only the Fe (oxyhydr)oxides of interest (goethite and hematite, as identified by high-resolution SEM) and none of the mineralogical impurities. The natural sample, NatM1, is a coarse-grained, mineralogically pure magnetite, which originates from a site of active Fe ooid deposition off Panarea, one of the volcanic islands of the Aeolian Arc (Tyrrhenian Sea, Italy). This magnetite displays high Ti concentrations (Fig. A24).

The natural case study samples (App01 and App02) were measured as round 1" polished sections. The sections were prepared by immersing the samples in epoxy resin poured into a 1" round plastic mold. Samples were stuck to double-sided tape during immersion to prevent them from moving. The samples were left to dry for 24 hours, after which the section was polished to expose as much of the submerged sample as possible, and until the desired smoothness was achieved (usually <1 μm).

FTIR results

Goethite is positively identified (Fig. A5A) by O-H stretching at ≈3100 cm^{-1}, in-plane O-H bending at ≈890 cm^{-1}, out-of-plane O-H bending at ≈790 cm^{-1}, and Fe-O stretching parallel to

unit cell axis 'a' at ≈610 cm^{-1} (Schwertmann and Cornell, 1991). Hematite is positively identified (Fig. A5B) by two Fe-O vibrational mode absorption bands at ≈430 and ≈530 cm^{-1}, which are perpendicular to the 'c' direction (Rendon and Serna, 1981). In addition, a broad 660-1200 cm^{-1} band composite is observed in all hematite spectra, which has previously been attributed to sorbed compounds (e.g., Hug, 1997). None of these previously suggested compounds were present in our samples, suggesting that other mechanisms are responsible for this band composite.

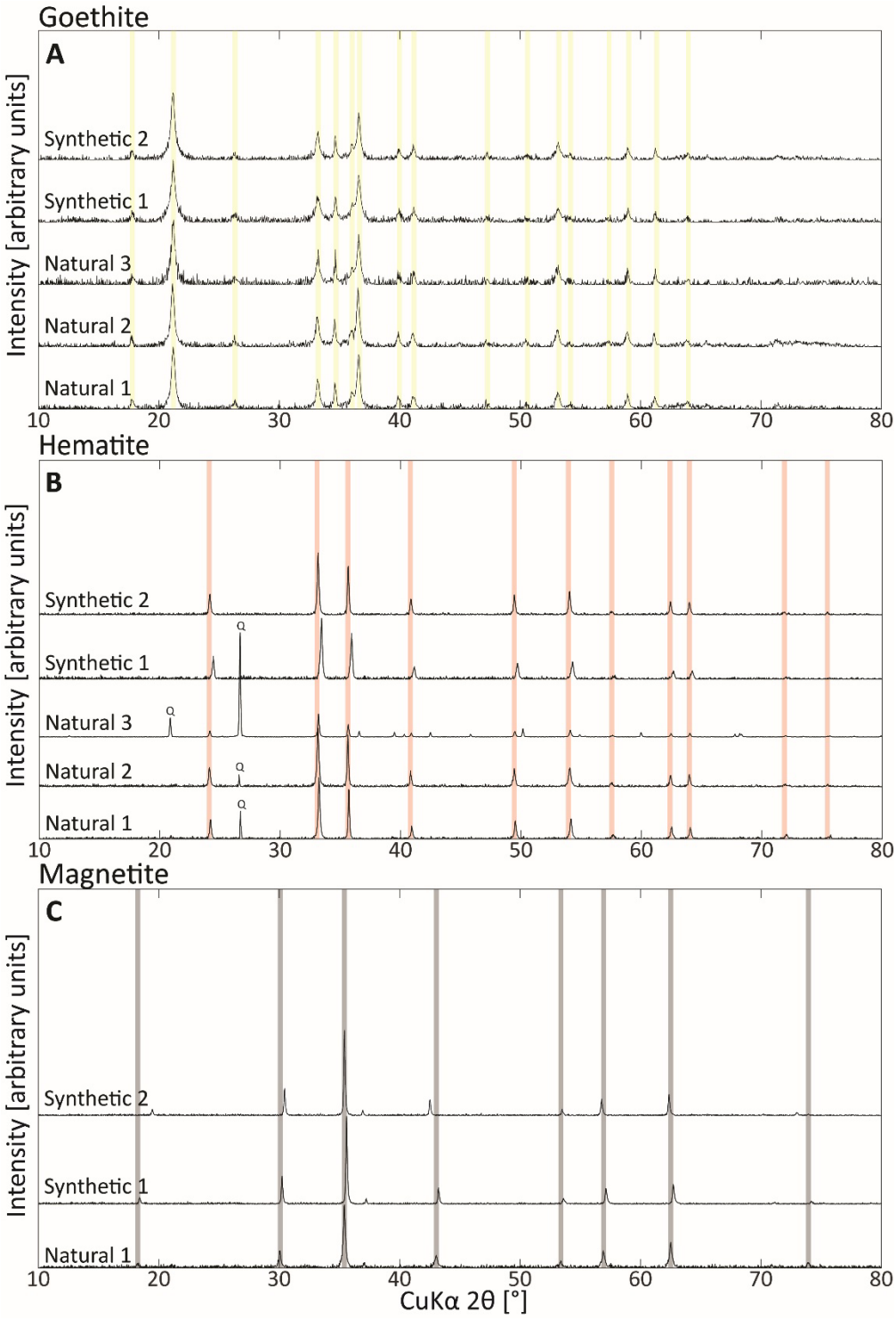

Figure A1. X-ray diffractograms of natural and synthetic Fe oxides and oxyhydroxides explored in this study. Color bars mark selected diffraction features taken from the International Centre for Diffraction Data (ICDD) database. The natural hematite samples contain minor amounts of quartz (SiO_2), which is denoted by 'Q'.

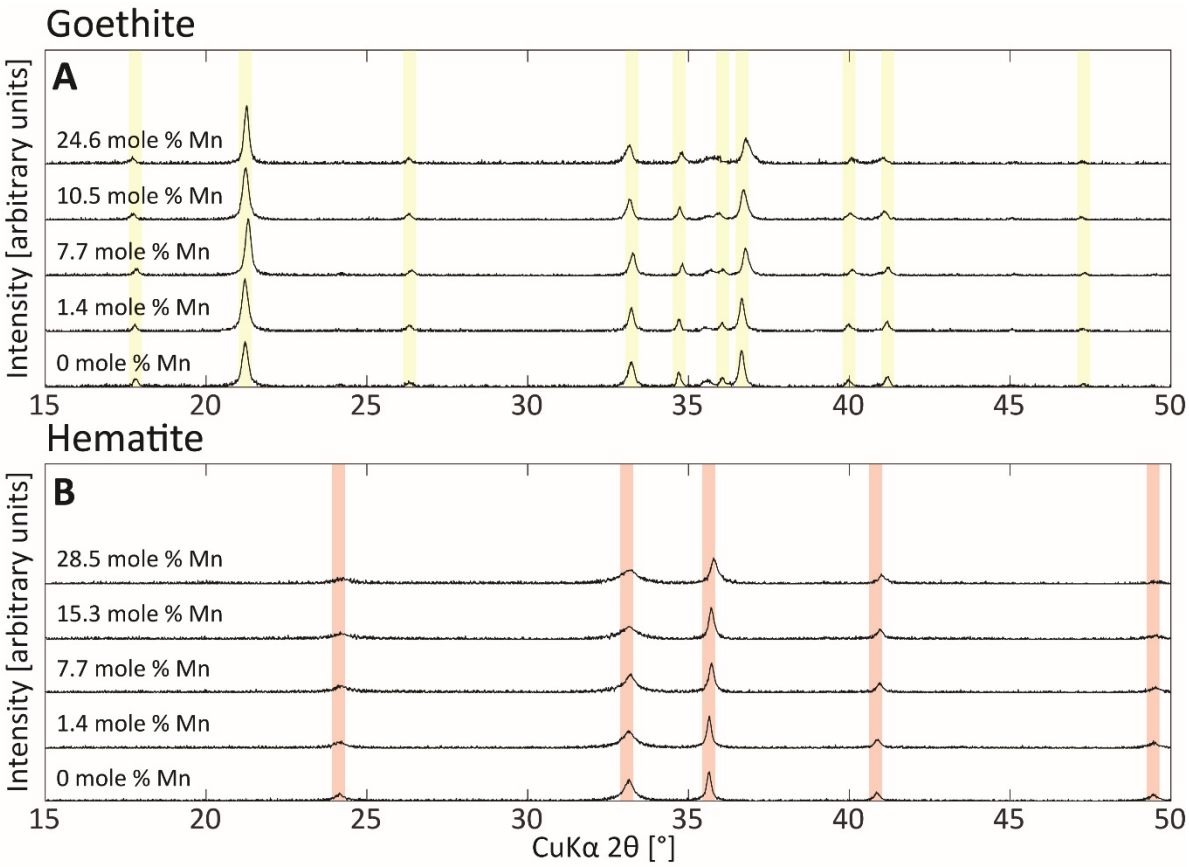

Figure A2. X-ray diffractograms of Mn-substituted hematite and goethite. No phases other than hematite and goethite could be detected. Color bars mark selected diffraction features taken from the International Centre for Diffraction Data (ICDD) database.

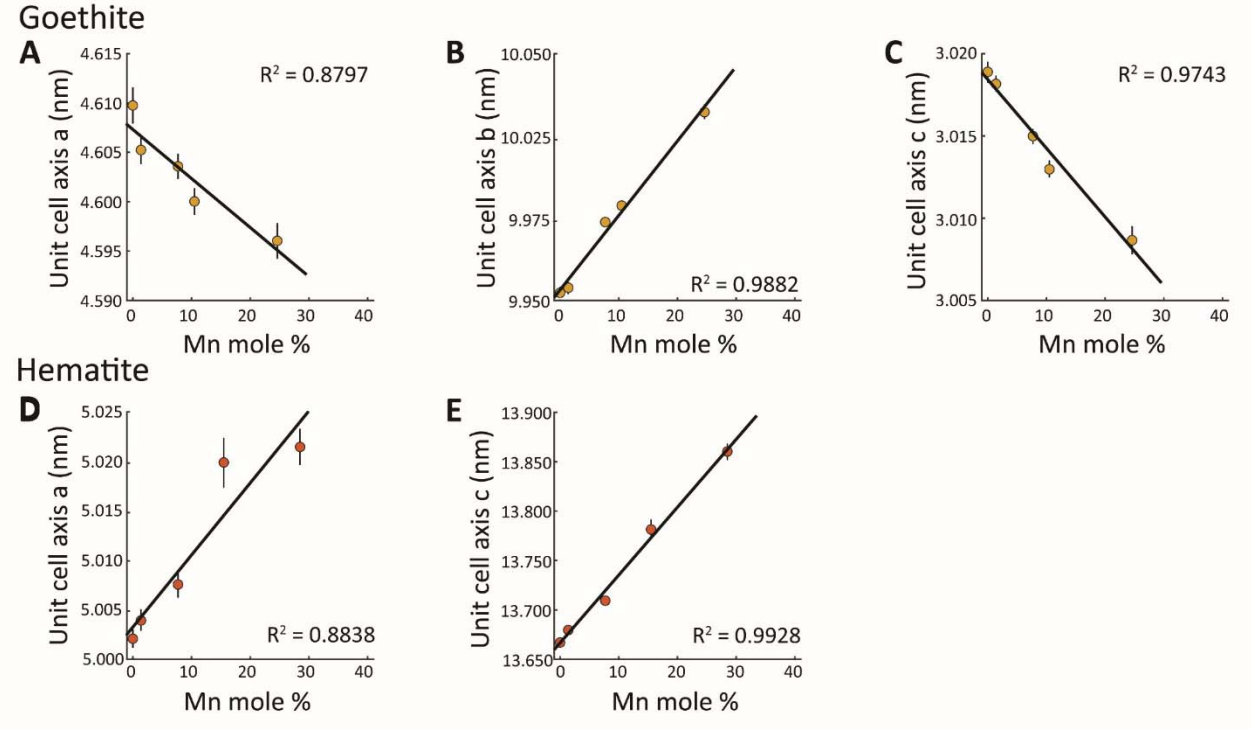

Figure A3. The effect of Mn substitution for Fe on goethite and hematite unit cell dimensions. (A) Goethite 'a' axis, (B) goethite 'b' axis, (C) goethite 'c' axis. (D) Hematite 'a' axis, (E) hematite 'c' axis. Error bars represent one standard deviation (1σ) on the cell axis dimensions extracted from the X-ray diffractograms (Table 1). R^2 is used to illustrate the linear relationship between the goethite and hematite unit cell dimensions and the amount of Mn substitution for Fe, despite the relatively small sample size (n=5), which may lead to unreliable statistics (see Jenkins and Quintana-Ascencio, 2020).

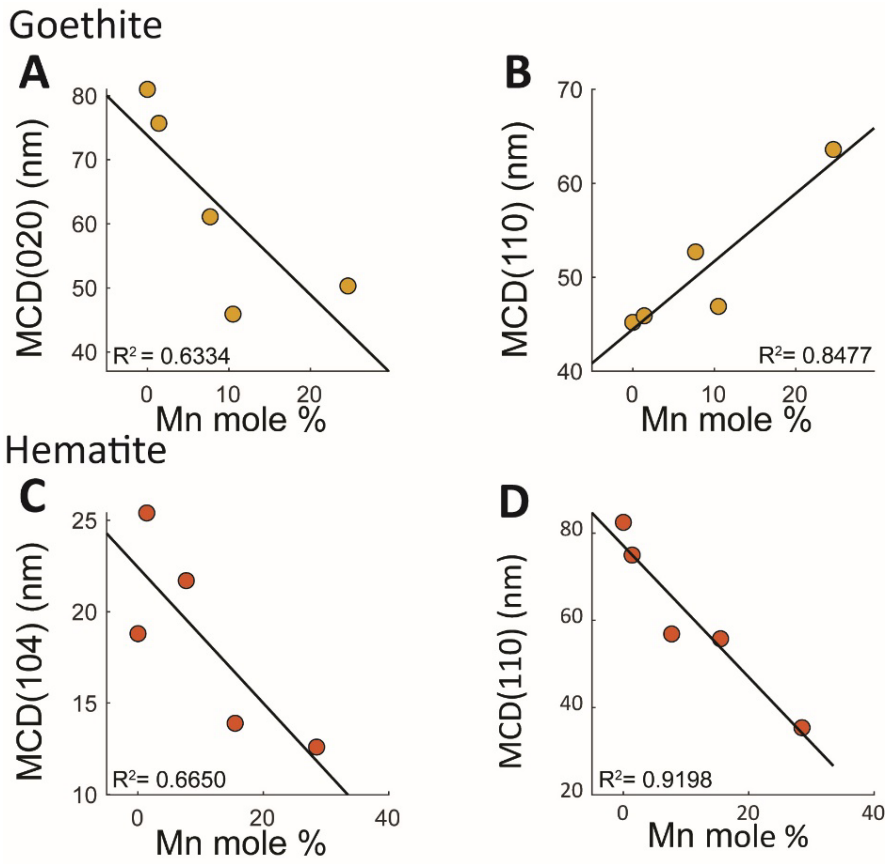

Figure A4. The relationship between Mn substitution in goethite (panel A & B) and hematite (panels C & D) and the Mean Crystallite Dimension (MCD). For goethite, MCD (110) was used to represent the crystal size along the 'a' axis, while MCD (020) was used to represent the crystal size in the 'b' axis. For hematite, MCD (104) was used to represent the crystal size along the 'c' axis, while MCD (110) was used to represent the crystal size in 'a'-'b' plane. R^2 is used to illustrate the linear relationship between the goethite and hematite unit cell dimensions and the amount of Mn substitution for Fe, despite the relatively small sample size (n=5), which may lead to unreliable statistics (see Jenkins and Quintana-Ascencio, 2020).

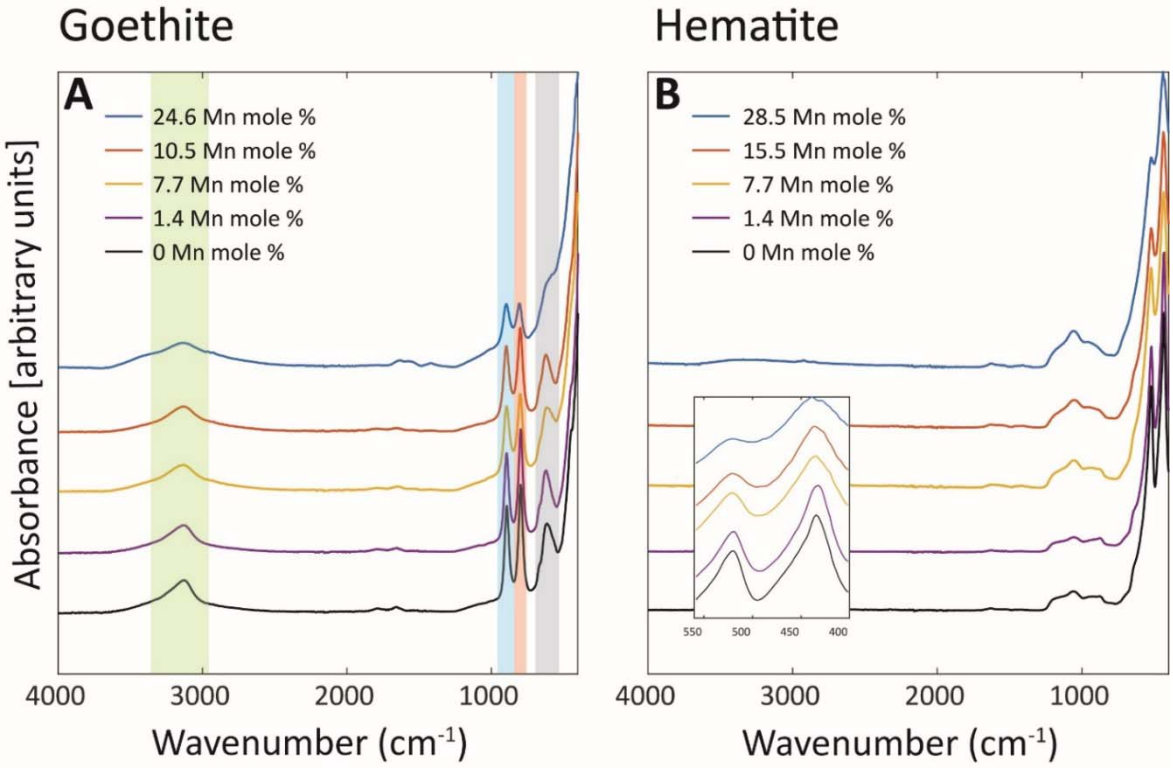

Figure A5. FTIR spectra of Mn-substituted (A) goethites and (B) hematites. Compared to available Fe oxide and oxyhydroxide FTIR spectra (Cornell and Schwertmann, 2003), our results confirm the mineralogy of our samples. For goethite, the bulk O-H stretching is highlighted by a light green rectangle (≈3100 cm^{-1}), and the in-plane (≈890 $cm^{-}1$) and out-of-plane (790 $cm^{-}1$) OH bending is highlighted by the blue and red colored rectangles, respectively. The light gray rectangle marks the Fe-O stretch parallel to unit cell axis a (≈610 cm^{-1}). For hematite, the inset window presents two Fe-O vibrational mode absorption bands (≈430 and ≈530 cm^{-1}), which are perpendicular to the 'c' direction (Rendon and Serna, 1981). In addition, a broad 660-1200 cm^{-1} band composite of two shoulders at each end is observed in all hematite spectra. All goethite and hematite absorption bands become wider with increasing Mn substitution for Fe, as expected from the associated increase in the diversity of O-H and Fe-O bonding environments.

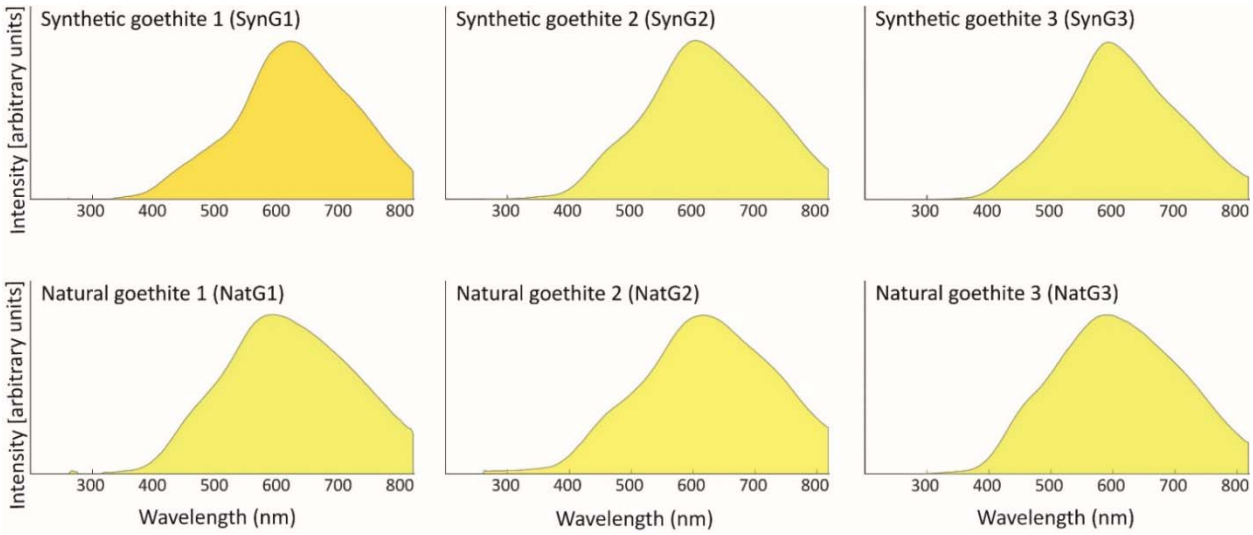

Figure A6. SEM-CL spectra of synthetic and natural goethite. The color under individual spectra represents their true color representation.

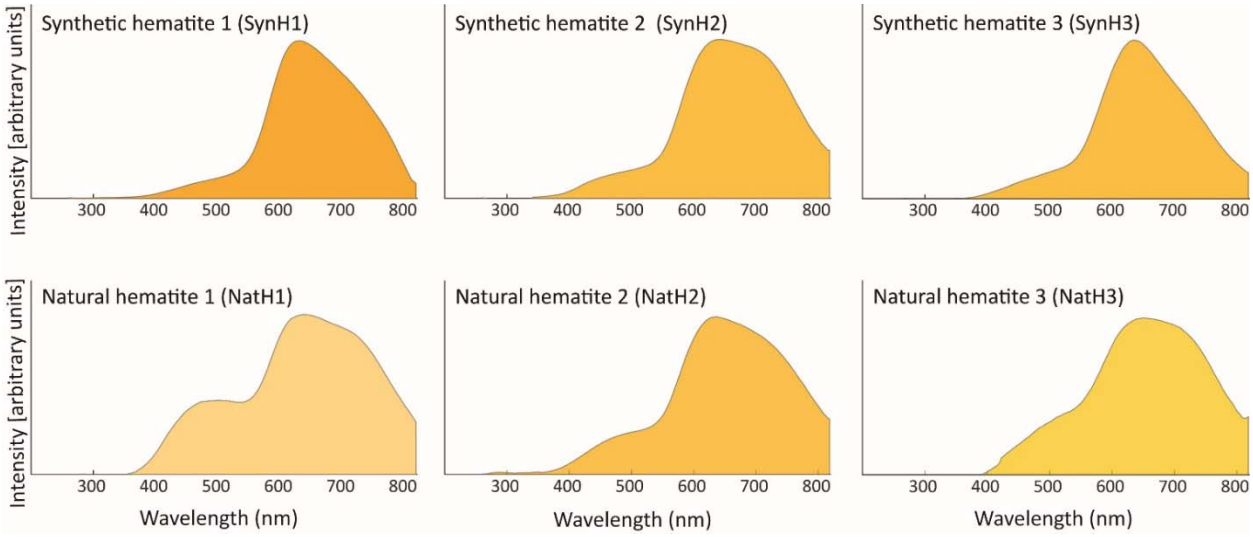

Figure A7. SEM-CL spectra of synthetic and natural hematite. The color under individual spectra represents their true color of emission.

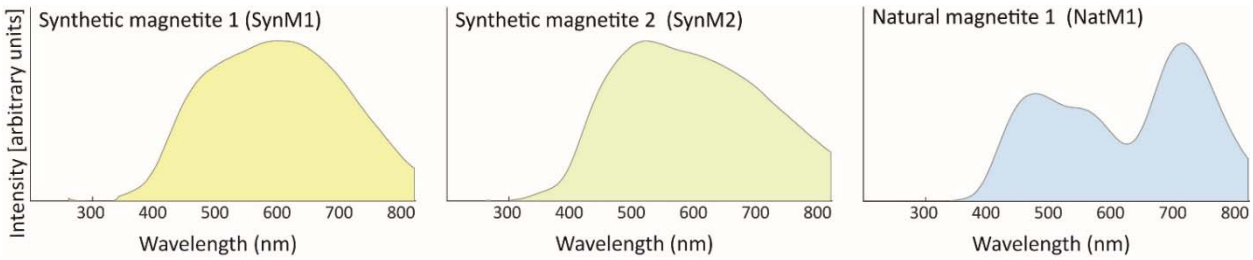

Figure A8. SEM-CL spectra of synthetic and natural magnetite. The color under individual spectra represents their true color of emission.

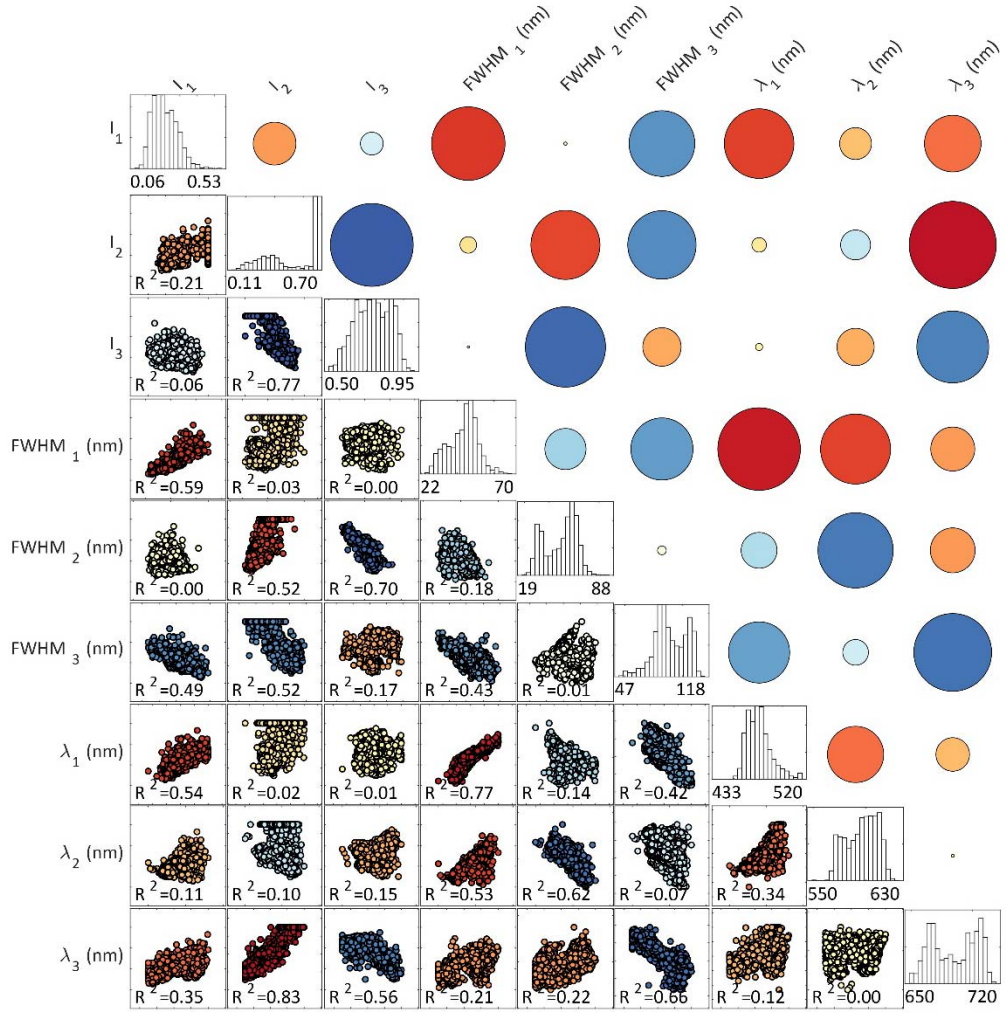

Figure A9. Correlation matrix of goethite spectral parameters, as obtained by deconvolution of individual spectra into Gaussian emission bands. The diagonal shows the distribution of the spectral parameter, with minimal and maximal values shown below the histograms (on the left and right, respectively). The lower diagonal elements show scatter plots of pairs of parameters, with the marker color representing the sign (red=positive, blue=negative) and strength (–1 to 1) of the correlation. The squared Pearson's correlation coefficient (R^2) is shown in the lower left corners of panels. The circles in the upper diagonal elements are colored and sized according to the sign and absolute value of the strength of the correlation, respectively.

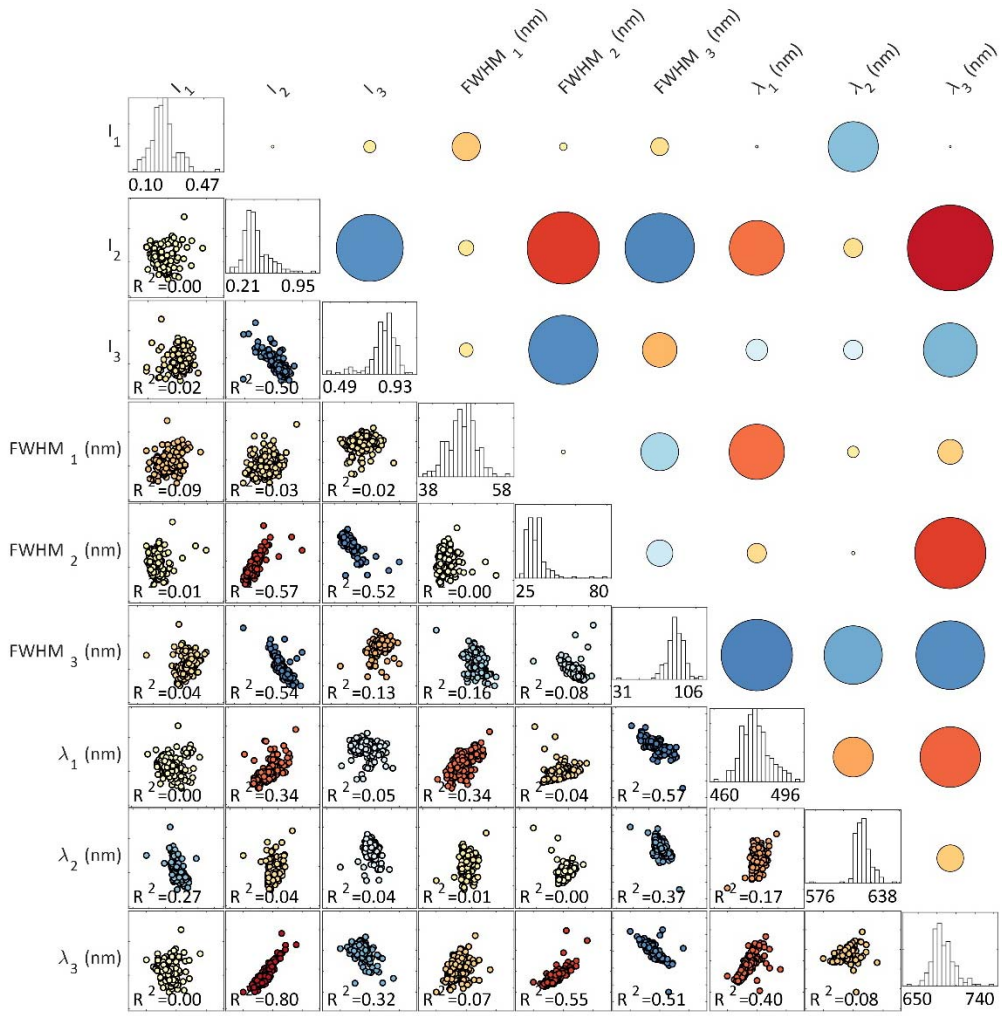

Figure A10. Correlation matrix of hematite spectral parameters, as obtained by deconvolution of individual spectra into Gaussian emission bands. The diagonal shows the distribution of the spectral parameter, with minimal and maximal values shown below the histograms (on the left and right, respectively). The lower diagonal elements show scatter plots of pairs of parameters, with the marker color representing the sign (red=positive, blue=negative) and strength (–1 to 1) of the correlation. The squared Pearson's correlation coefficient (R^2) is shown in the lower left corners of panels. The circles in the upper diagonal elements are colored and sized according to the sign and absolute value of the strength of the correlation, respectively.

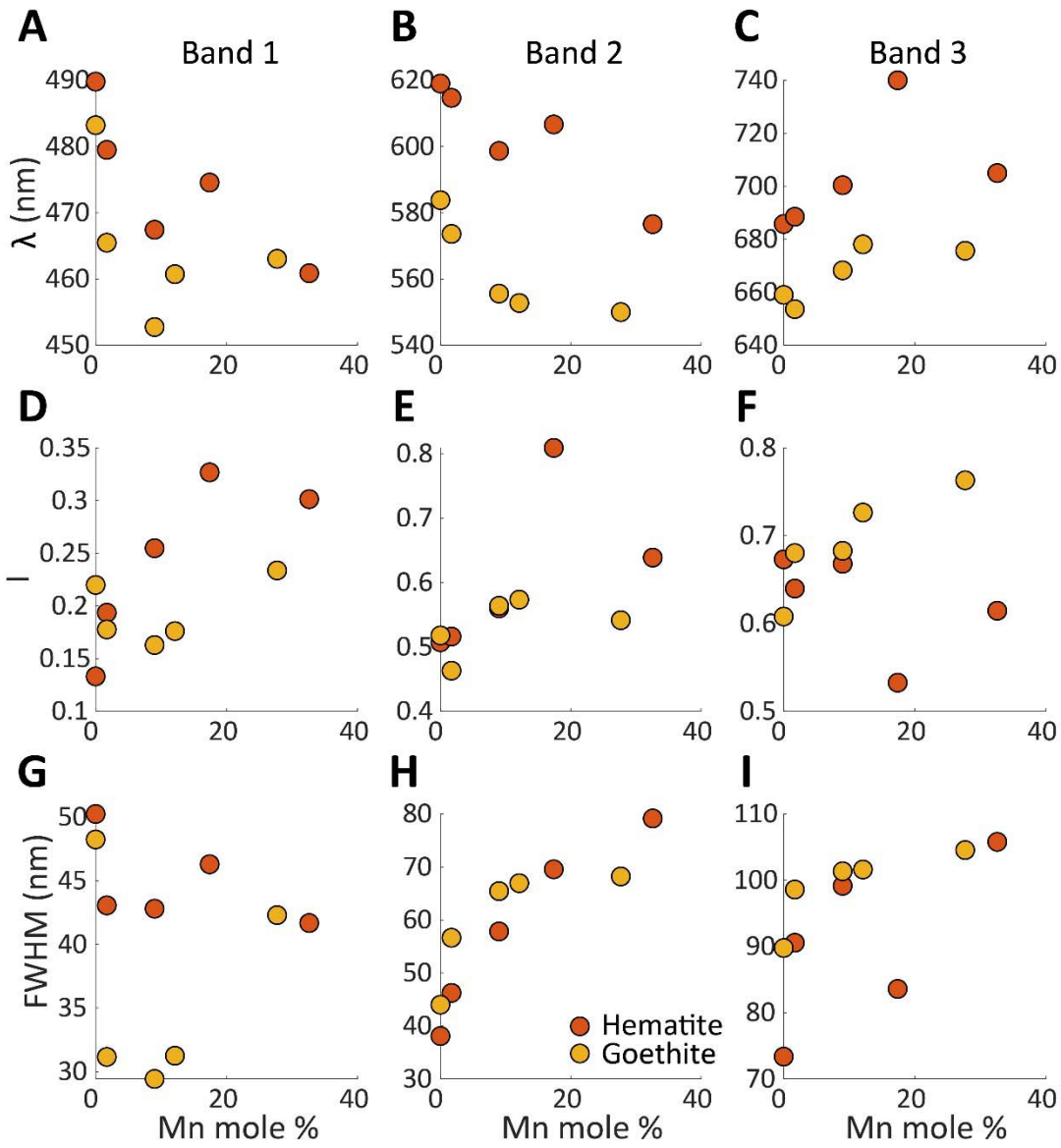

Figure A11. Emission band properties as a function of Mn concentration (mole %) in synthetic goethite and hematite. For each band (1, 2, 3, in the three columns), the wavelength of peak emission (λ in nm, row 1), the normalized intensity (I in arbitrary units, row 2) and the full-width at half-maximum (FWHM in nm, row 3) are shown.

Mineral	Serial number
Goethite	01-072-8206
Hematite	01-076-9683
Quartz	01.074-1811
Kaolinite	01-078-1996
Dolomite	COD 1200014
Calcite	00-005-0586

Figure A12. Legend for X-ray diffraction data from natural case studies. Peaks in diffractograms from the the Rapitan iron formation (Fig. A17) and the Agbaja ooidal ironstone (Fig. A13) are colored according to this legend.

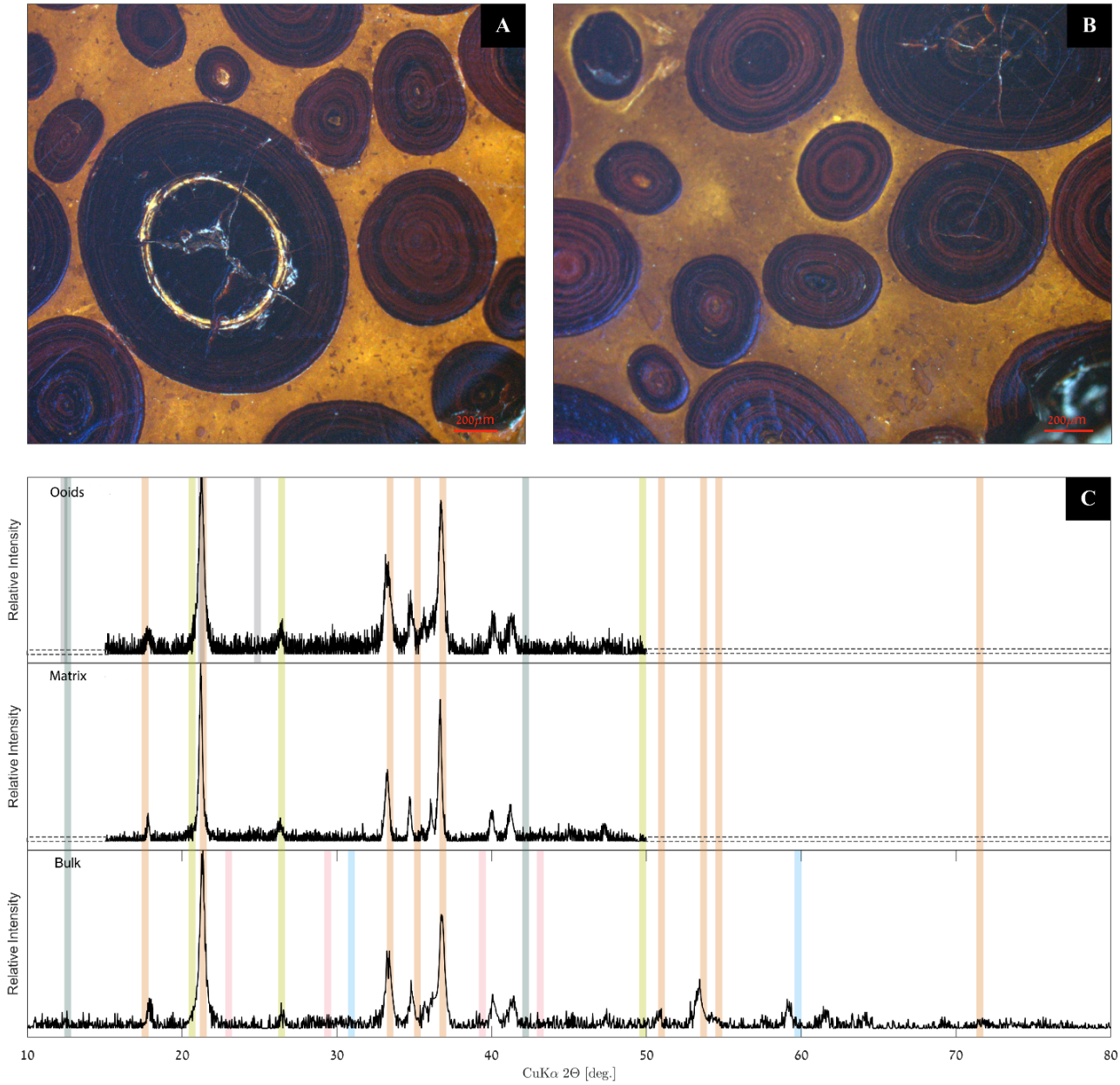

Figure A13. Petrography and mineralogy of the Agbaja ooidal ironstone (App01). (A, B) Reflected plane-polarized light photomicrograph. (C) X-ray diffractograms, which were automatically compared with the International Center for Diffraction Data (ICDD) database and the Crystallography Open Database (COD). Individual diffraction peaks are colored according to the legend in Fig. A12.

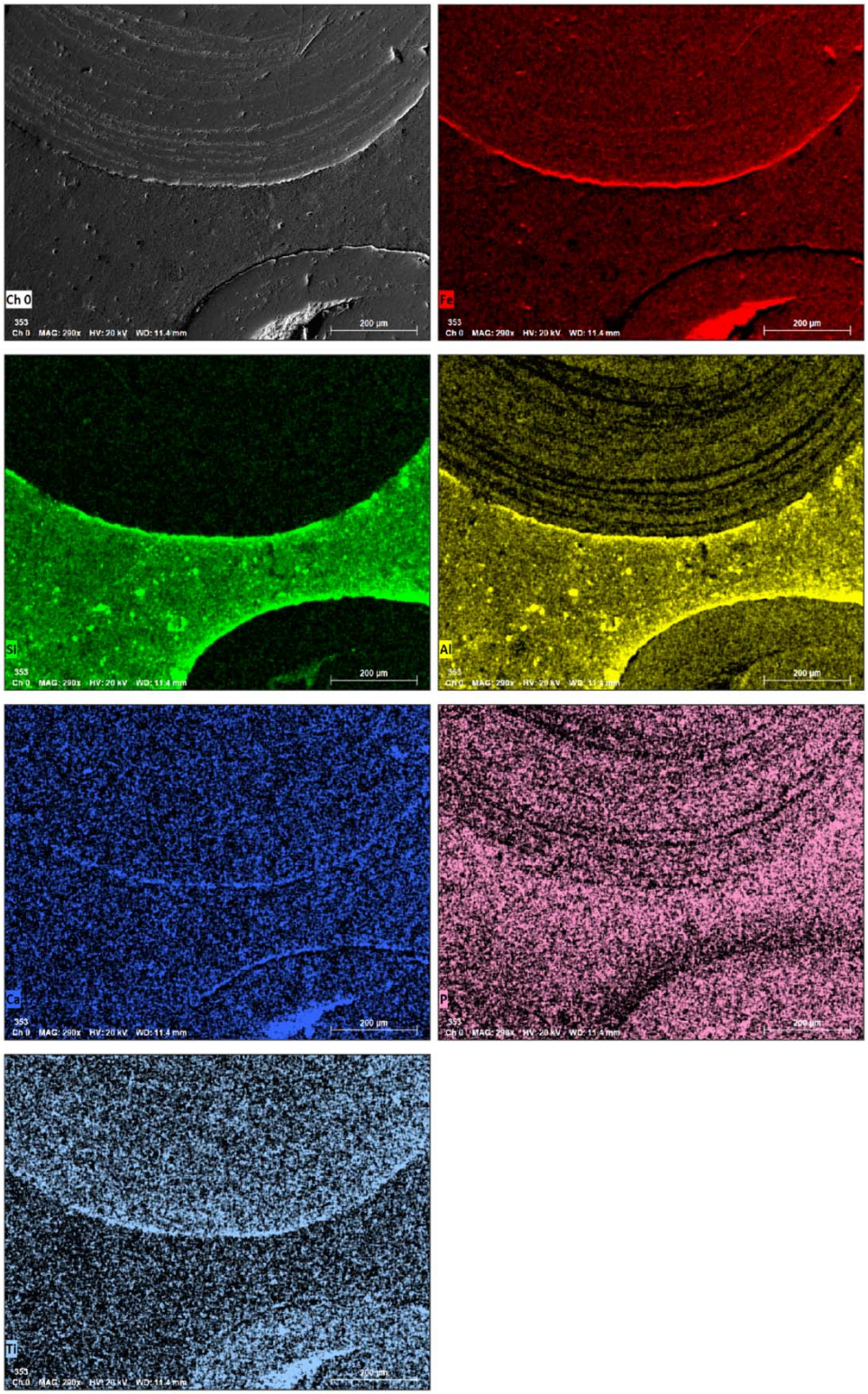

Figure A14. Elemental maps (SEM-EDS) of goethite ooids from the Agbaja ooidal ironstone (App01), embedded in a goethite matrix.

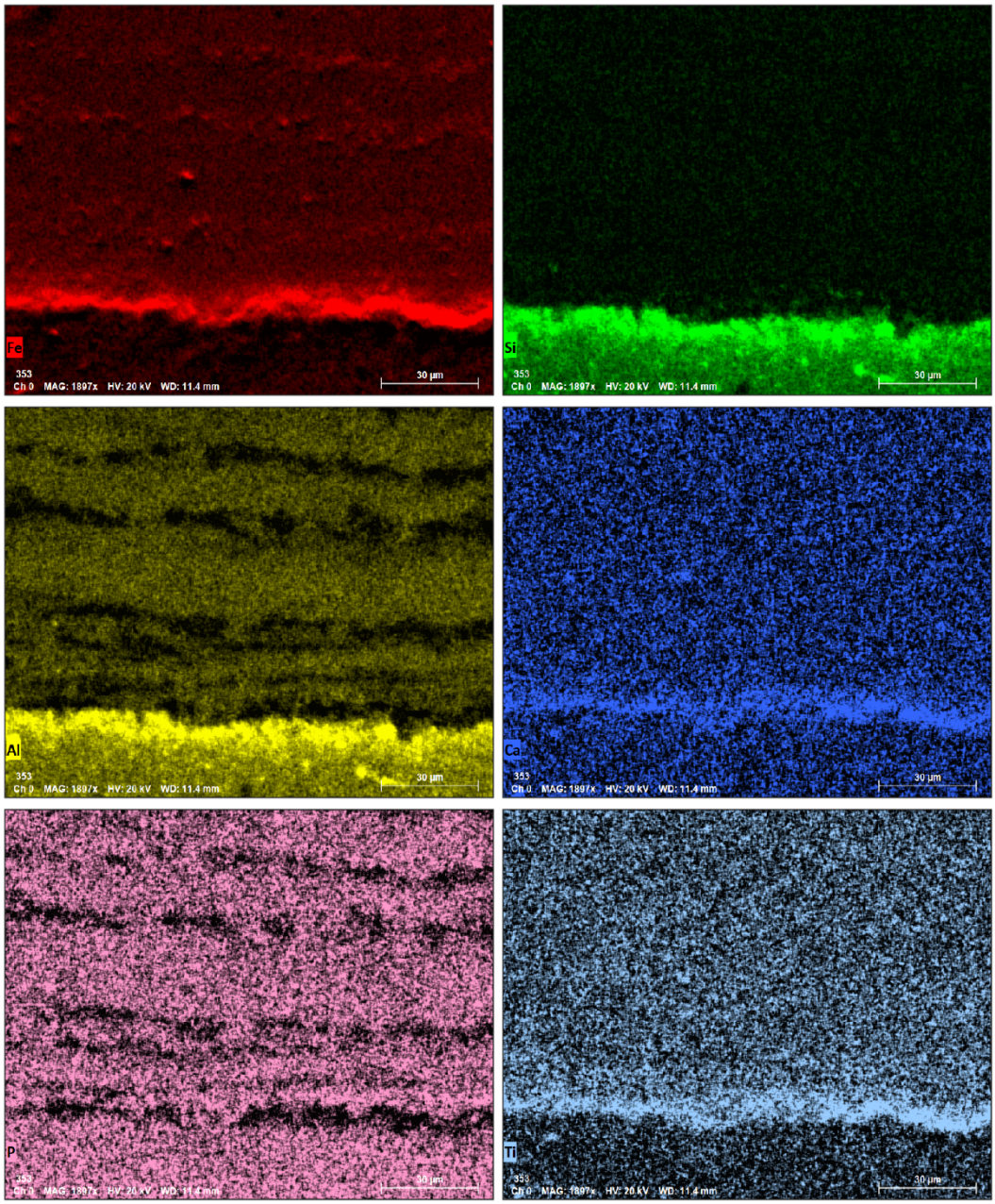

Figure A15. Elemental maps (SEM-EDS) zoomed in on the transition between a goethite ooid and the goethite matrix in the Agbaja ooidal ironstone (App01).

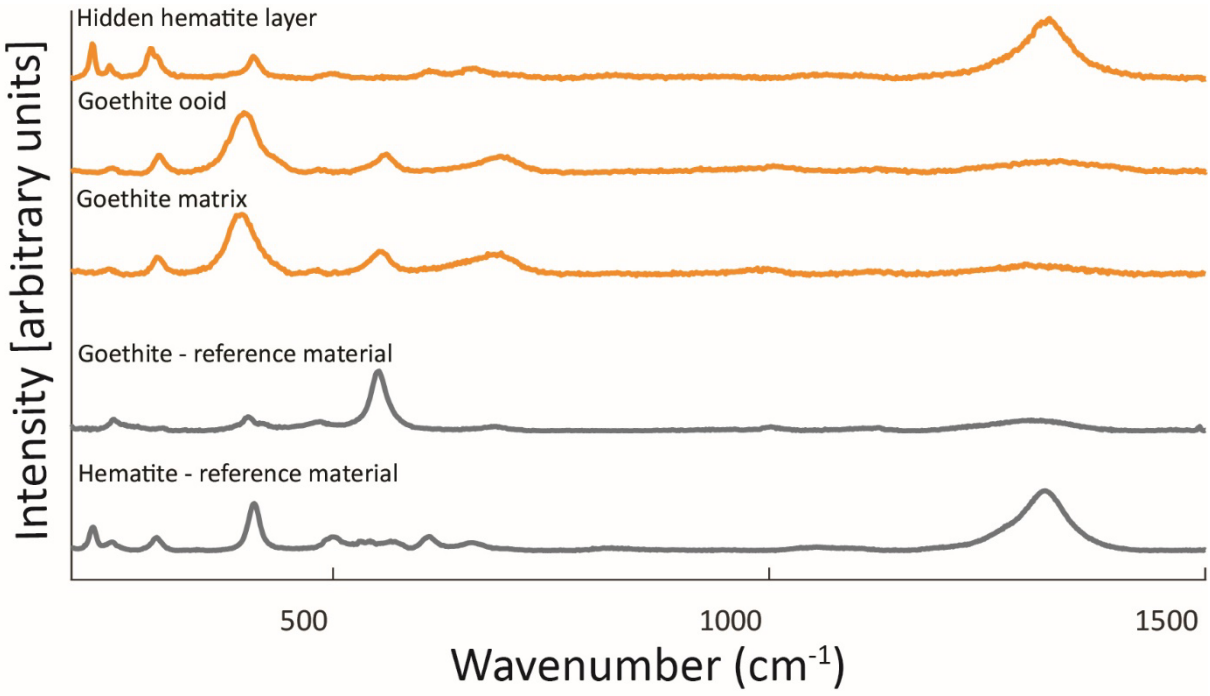

Figure A16. Raman spectra of different regions of interest of the Agbaja ooidal ironstone (App01) compared to reference hematite and goethite spectra. In accordance with the SEM-CL analysis, the Raman spectra indicate that the ooids and matrix are both composed of goethite, and that the ooids contain thin layers of hematite that were not detected by XRD.

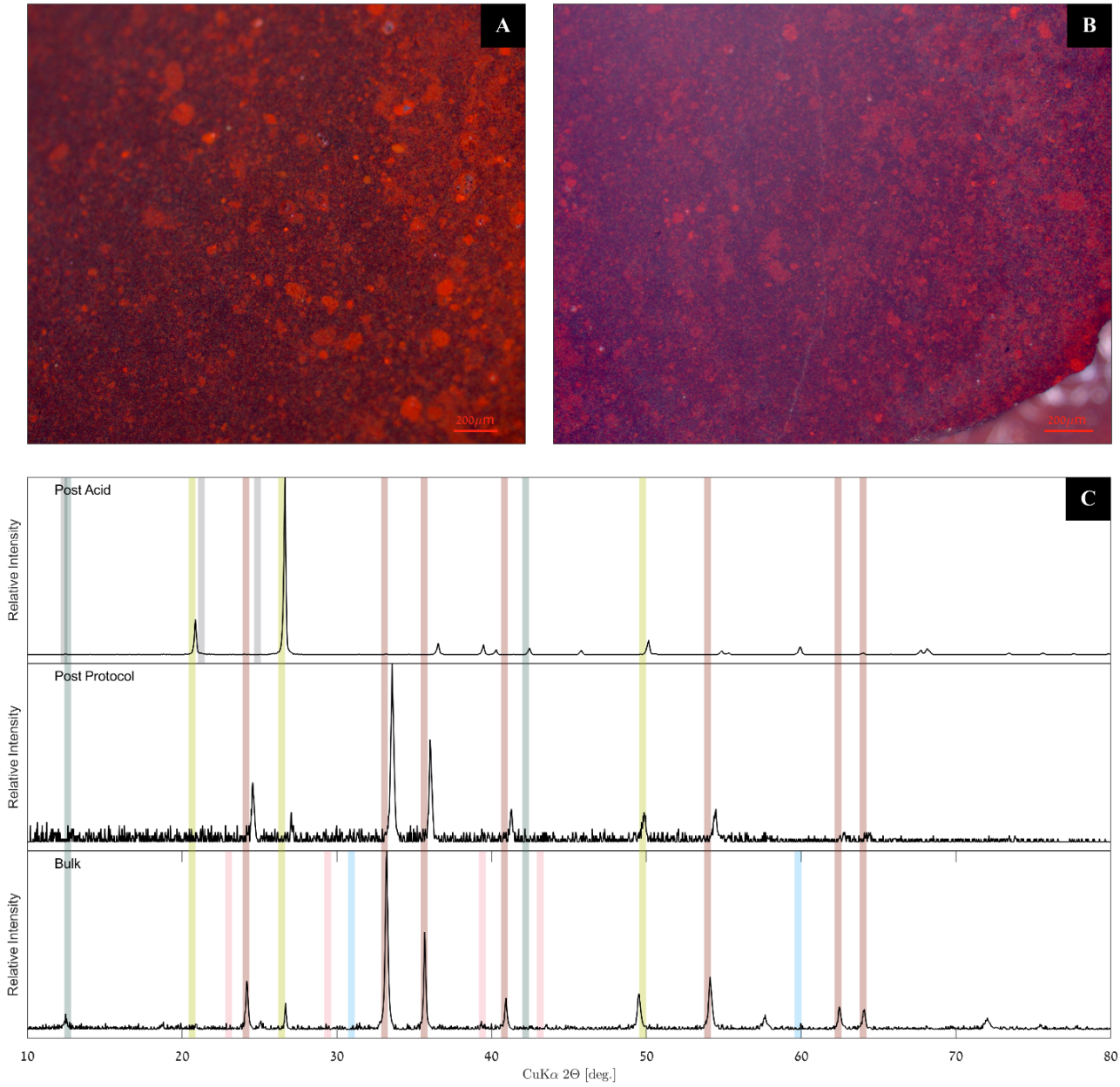

Figure A17. Petrography and mineralogy of the Rapitan iron formation (App02). (A, B) Reflected plane-polarized light photomicrograph. (C) X-ray diffractograms, which were automatically compared with the International Center for Diffraction Data (ICDD) database and the Crystallography Open Database (COD). Individual diffraction peaks are colored according to the legend in Fig. A12.

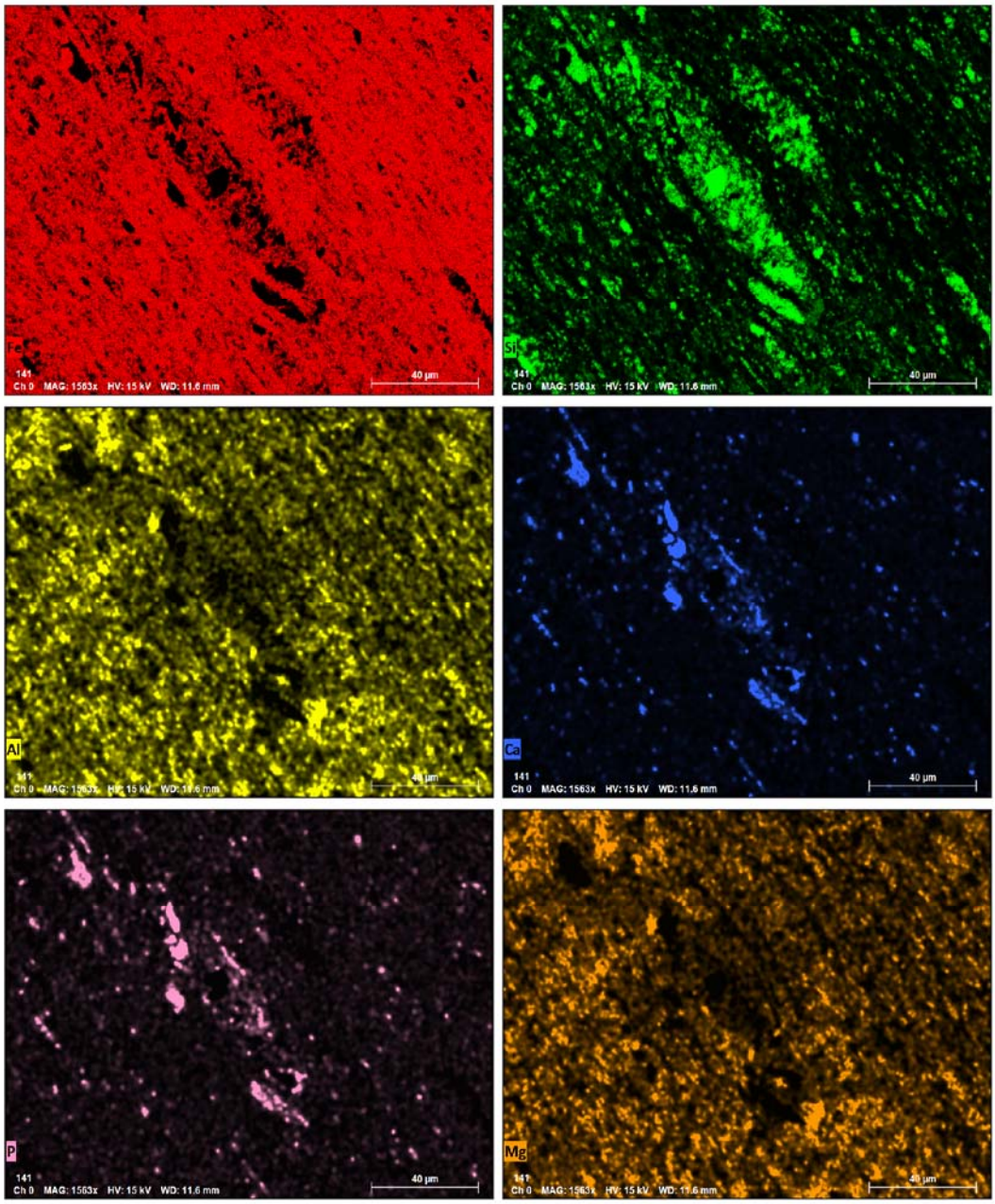

Figure A18. Elemental maps (SEM-EDS) of the Rapitan iron formation (App02). The sample consists mostly of hematite and Fe-rich quartz (jasper).

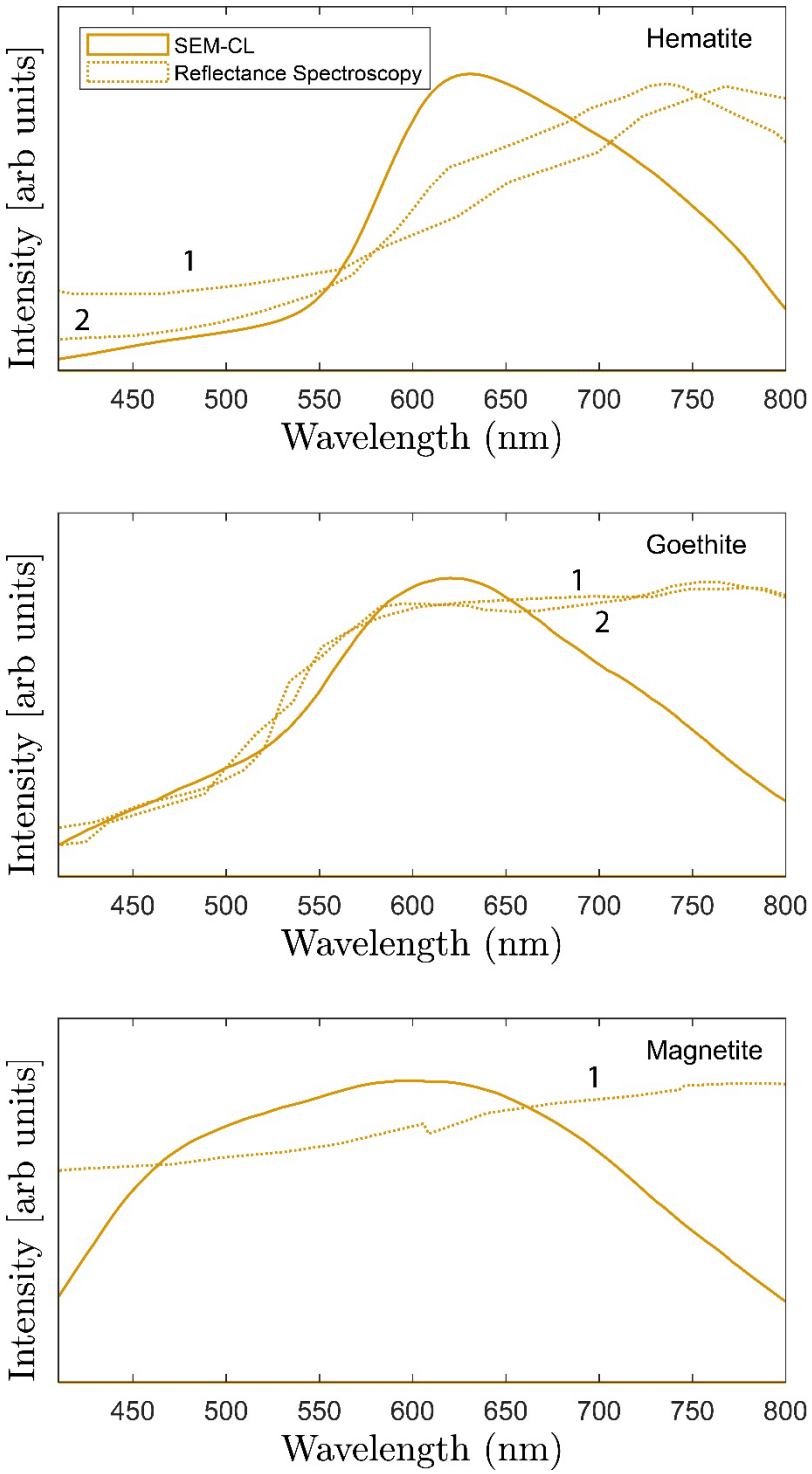

Figure A19. Comparison of SEM-CL and visible and near-infrared reflectance spectra of hematite, goethite and magnetite. References for hematite reflectance spectra: (1) Torrent and Barron (2002); (2) Moris et al. (1985). References for goethite reflectance spectra: (1) Torrent and Barron (2002); (2) Moris et al. (1985). References for magnetite reflectance spectra: (1) Moris et al. (1985). SEM-CL spectra were taken from synthetic samples of each mineral (synthetic hematite 1, synthetic goethite 1, and synthetic magnetite 1).

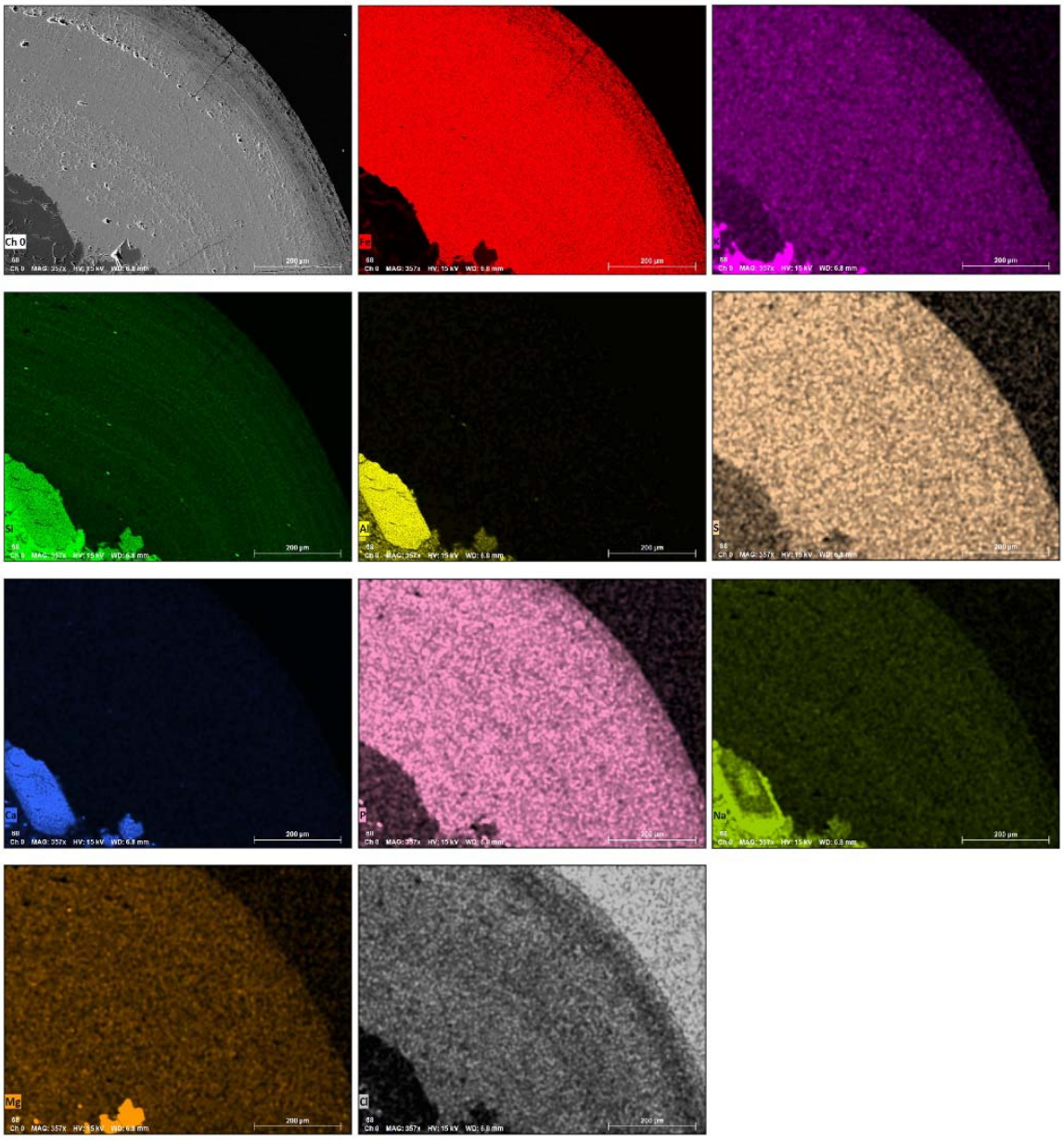

Figure A20. Elemental maps (SEM-EDS) of natural goethite 1 (NatG1). Ooids are composed of concentric accretionary layers of poorly crystalline Fe hydroxides, some of which have aged into goethite, and amorphous silica, with an andesitic rock core. No other minerals are detected by XRD, suggesting that elements other than Fe and Si observed in the ooid layers do not form additional mineral phases, but may be sorbed or substituted into one of the phases detected in the sample. These elements come from the mixture of seawater and exhalative hydrothermal fluids rising through the marine substrate.

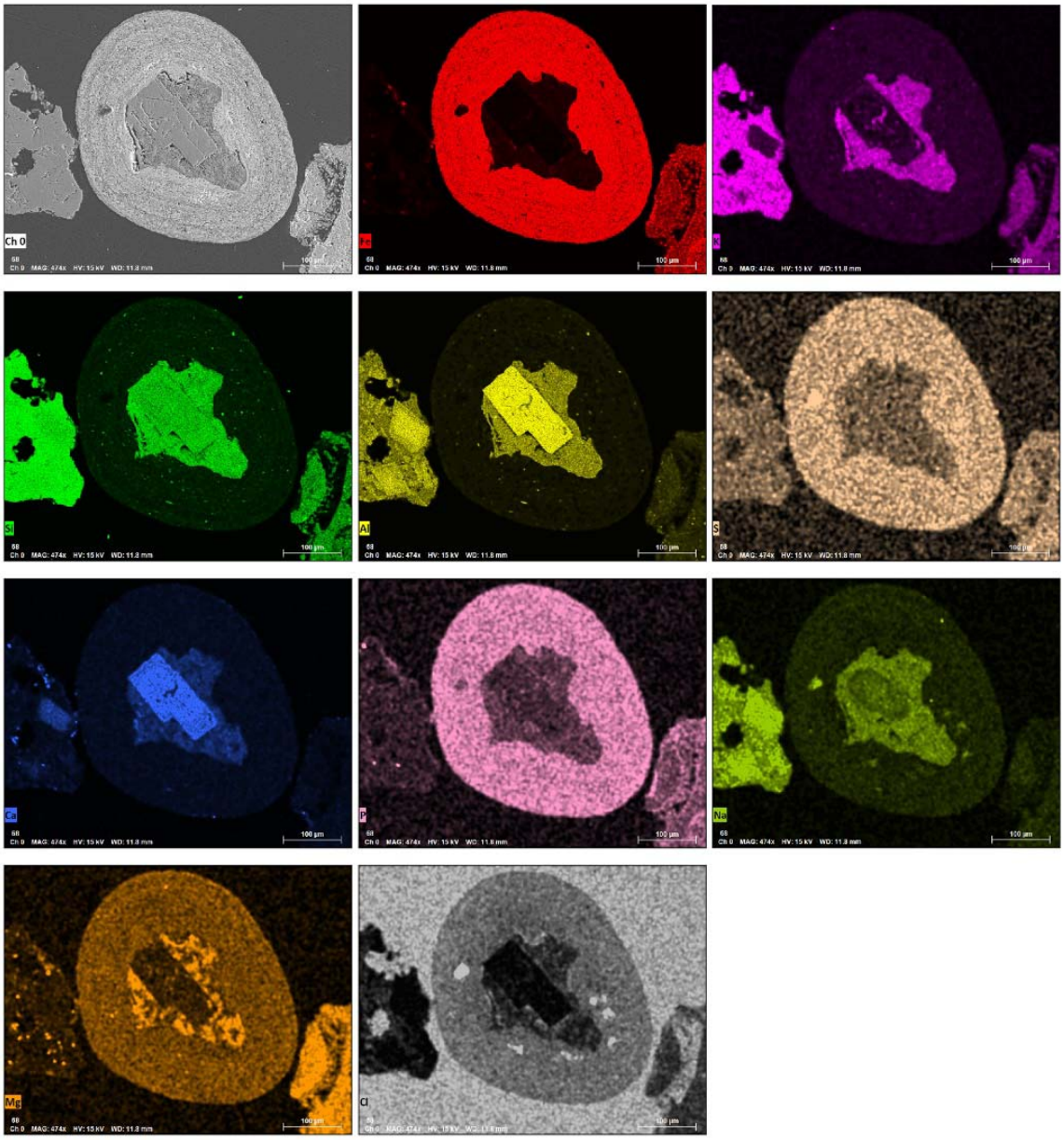

Figure A21. Elemental maps (SEM-EDS) of natural goethite 3 (NatG3). This goethite comes from ooids collected off Panarea, one of the volcanic islands of the Aeolian Arc (Tyrrhenian Sea, Italy), which are composed predominantly of goethite, with some minor poorly crystalline Fe hydroxides and silica. As with NatG1 (Fig. A19), elements other than Fe and Si in the ooid layers come from the mixture of seawater and exhalative hydrothermal fluids rising through the marine substrate, which is rich in fragments of volcanic rocks. Evident also is a Ca-Na-Al-silicate rock core, overgrown by a Mg-K-Na-Al-silicate, and then by the (oxyhydr)oxides.

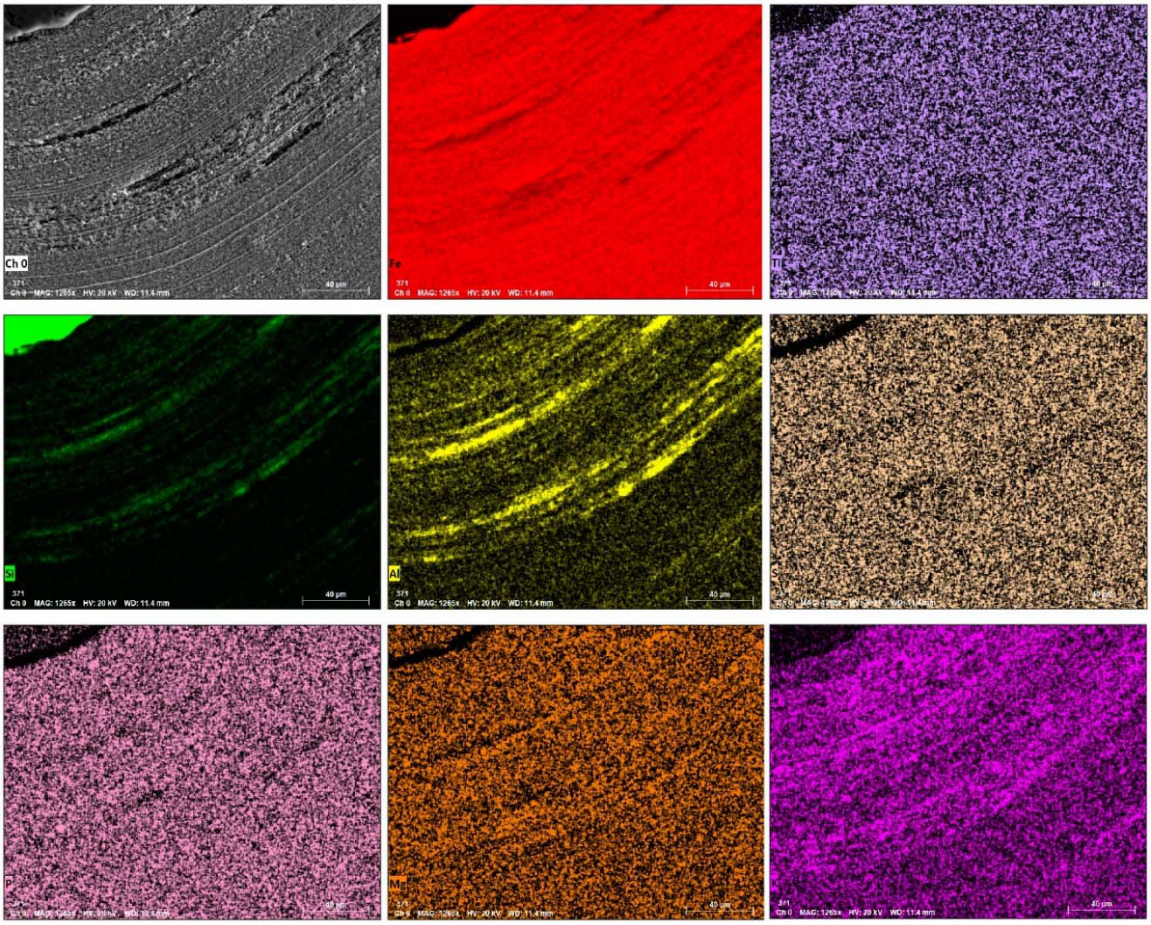

Figure A22. Elemental maps (SEM-EDS) of natural hematite 1 (NatH1). This sample is from the oolitic Chuanlinggou Formation, which belongs to the Changcheng Group, the oldest sedimentary succession in the Yanshan basin, a continental rift that developed on the northern margin of the North China Block. The ooids are composed of hematite-rich layers and Al-rich silicate layers.

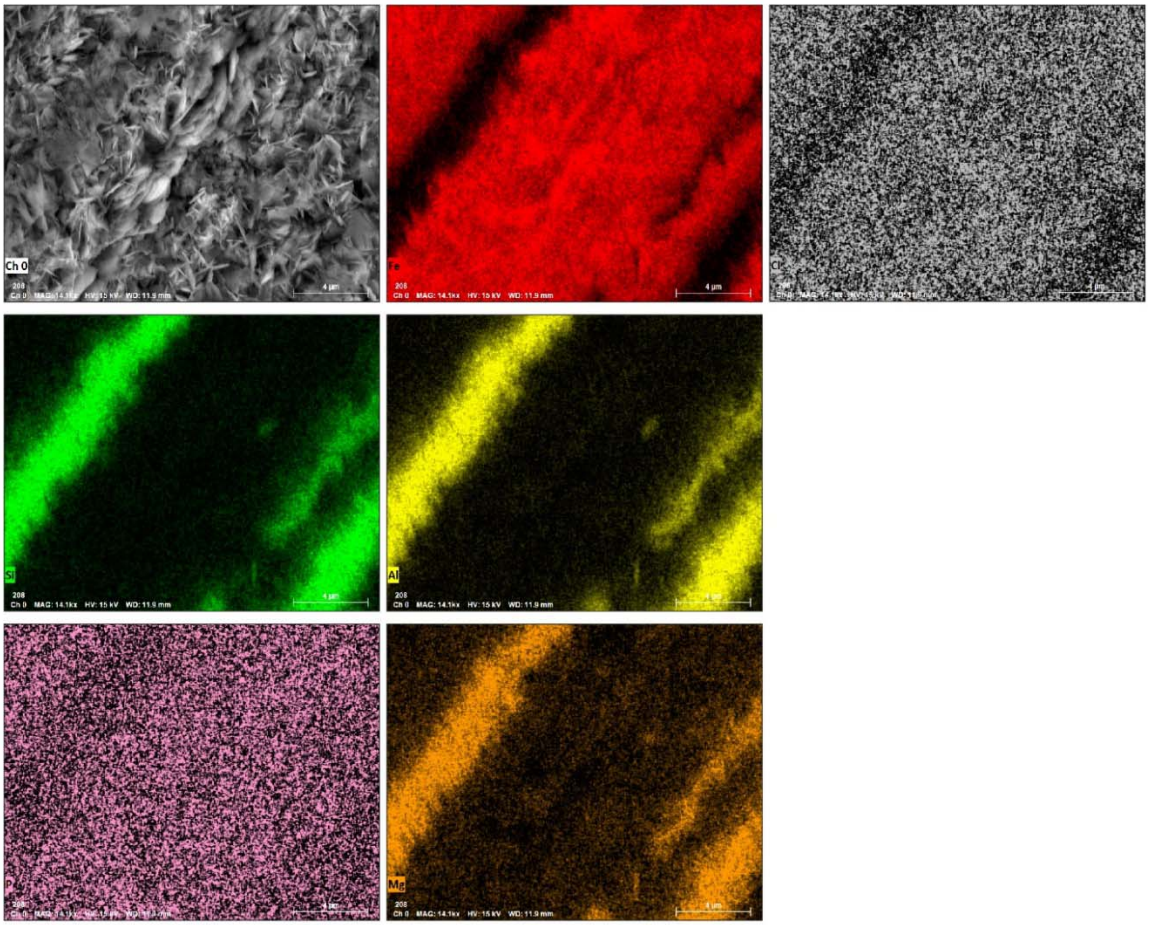

Figure A23. Elemental maps (SEM-EDS) of natural hematite 2 (NatH2). These hematite-rich ooids are from the Australian Sherwin Iron Formation. The sample displays alternating layers of hematite and Al-Mg-rich silicates.

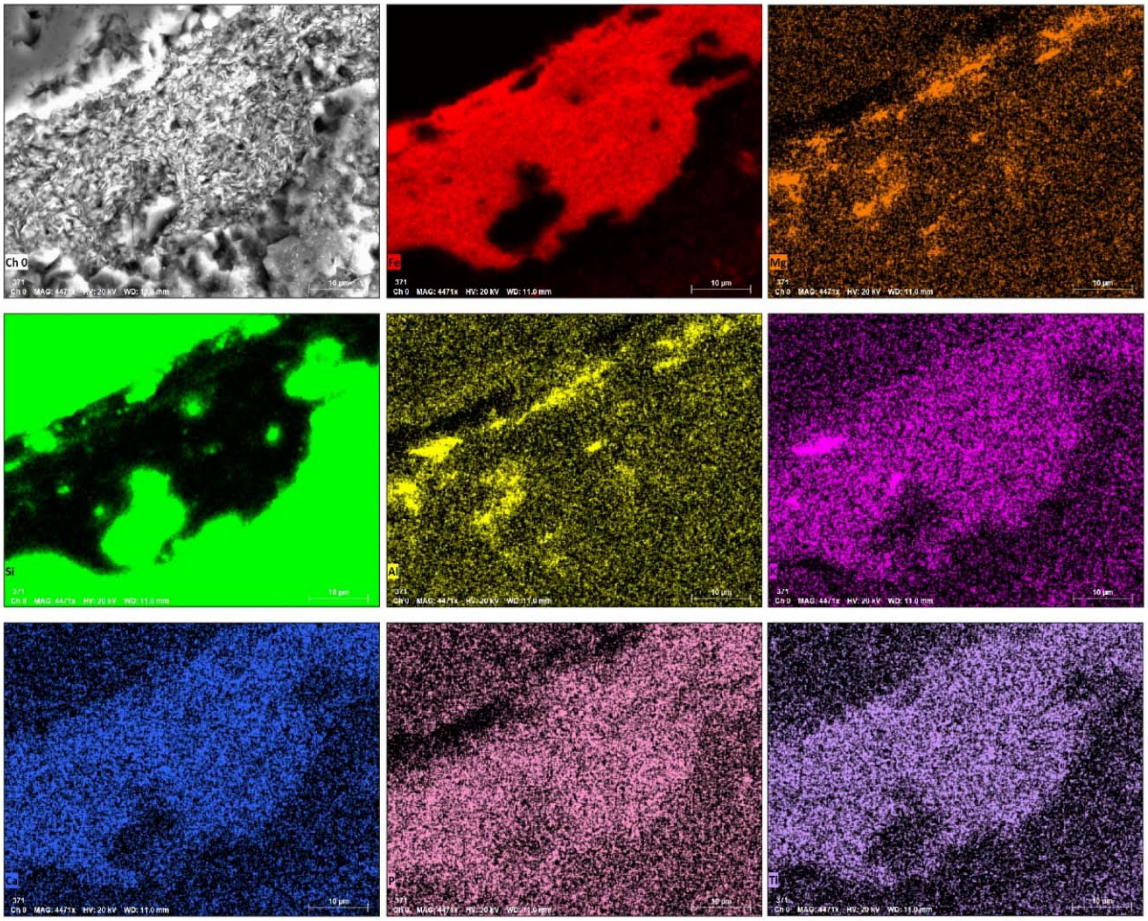

Figure A24. Elemental maps (SEM-EDS) of natural hematite 3 (NatH3). This sample is from the Gibraltar Formation. The formation is part of the Kahochella Group and is located in the East Arm of Great Slave Lake, Northwest Territories. The upper part of the Gibraltar Formation includes a granular iron formation, which contains granules of hematite set in fine-grained cherty cement.

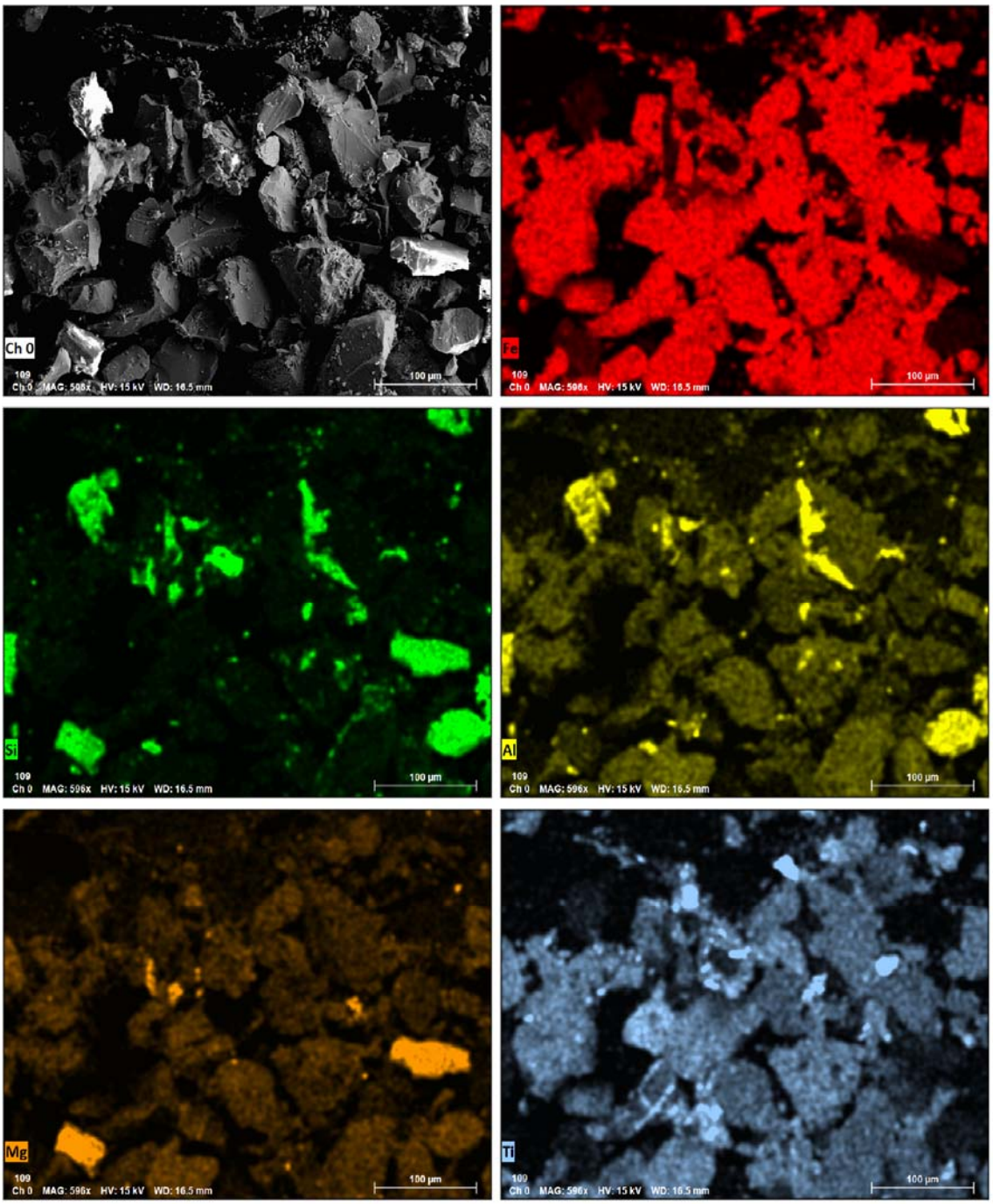

Figure A25. Elemental maps (SEM-EDS) of natural magnetite 1 (NatM1). This sample was collected off Panarea, one of the volcanic islands of the Aeolian Arc (Tyrrhenian Sea, Italy). The sample consists almost entirely of magnetite, with minor amounts of Mg and Al silicates.

Table A1. Description of natural samples included in this study. Ma: Millions of years before present. ka: Thousands of years before present.

Sample	Type	Depositional environment	Origin/formation
Natural hematite 1 (NatH1)	Round epoxy thick section	Intertidal marine	Chuanlingguo Formation, oolitic ironstone, ≈1650 Ma, Yanshan Basin, China
Natural hematite 2 (NatH2)	Round epoxy thick section	Shallow marine	Sherwin Ironstone, ≈1429-1492 Ma, Northern Territory, Australia
Natural hematite 3 (NatH3)	Round epoxy thick section	Shallow marine	The Gibraltar Iron Formation, ≈1880 Ma, Northwest Territories, Canada
Natural goethite 1 (NatG1)	Round epoxy thick section	Hydrothermally influenced marine	Modern marine ooids, ≈4.5 ka, Mahengetang, Indonesia
Natural goethite 2 (NatG2)	Pressed pellet	Pseudomorph after pyrite	Ferruginized sponges, Arava, Israel. Depositional age ≈65 Ma, pyrite oxidation age unknown.
Natural goethite 3 (NatG3)	Round epoxy thick section	Hydrothermally influenced marine	Modern marine ooids, Panarea, Aeolian Islands, Italy.
Natural magnetite 1 (NatM1)	Round epoxy thick section	Hydrothermally influenced marine or igneous	Ti-rich magnetite grains, Panarea, Aeolian Islands, Italy.

Table A2. Chemical composition of artificial seawater used to precipitate the synthetic magnetite sample SynM1.

Compound	$[Na^{+}]$ mmol/L	$[Cl^{-}]$ mmol/L	$[Mg^{2+}]$ mmol/L	$[SO4^{2-}]$ mmol/L	$[HCO_3]$ mmol/L	$[Fe^{3+}]$ mmol/L	$[Fe^{2+}]$ mmol/L
NaCl	420.3	420.3	—	—	—	—	—
$MgCl_2 \times 6H_2O$	—	99.8	49.9	—	—	—	—
$MgSO_4 \times 7H_2O$	—	—	0.1	0.1	—	—	—
SiO_2	—	—	—	—	—	—	—
$NaHCO_3$	10	—	—	—	10	—	—
$Fe(III)Cl_3 \times 6H_2O$	—	3	—	—	—	1	—
$Fe(II)Cl_2 \times 4H_2O$	—	3	—	—	—	—	1
Total concentration	430.3	526.1	50	0.1	10	1	1

Table A3. Chemical composition of synthetic iron oxides and oxyhydroxides studied and the Agbaja ironstone (ppm). Errors are at 1σ level. BDL – below detection limit.

	SynM1	SynM2	SynG1	SynG2	SynH1	SynH2	Agbaja ooids	Agbaja matrix
Mg	8.55±0.11	0.35±0.01	0.10±0.00	0.07±0.00	0.11±0.00	0.067±0.01	0.20±0.01	0.26±0.01
Al	12.4±1.68	3.17±0.99	3.44±2.60	2.15±0.88	1.68±0.72	1.52±0.67	29.8±3.13	23.9±4.13
P	BDL	BDL	BDL	BDL	BDL	BDL	10.4±0.58	8.62±0.95
Ti	0.90±0.23	0.76±0.07	0.84±0.00	0.30±0.01	0.71±0.11	1.25±0.05	1.55±0.10	0.46±0.07
Cr	0.22±0.00	0.16±0.00	0.19±0.00	0.08±0.00	0.16±0.00	0.16±0.00	0.09±0.00	0.05±0.00
Fe	717±1.41	735±8.67	634±10.3	700±5.23	682±8.18	711±2.31	683±6.87	627±2.51
Cu	0.13±0.00	0.08±0.00	0.02±0.00	0.01±0.00	0.14±0.00	0.16±0.00	0.02±0.00	0.02±0.00
Zn	2.26±0.04	0.76±0.01	0.07±0.01	0.01±0.00	0.09±0.00	0.16±0.01	0.18±0.00	0.19±0.01

Table A4. Chemical composition of Mn-substituted goethite and hematite (ppm). Errors are at 1σ level. BDL – below detection limit.

Mn (mol %)	0	1.4	7.7	10.5	15.3	24.6	28.5
Mg	0.55±0.04	BDL	BDL	0.04±0.00	0.46±0.02	BDL	BDL
Al	0.24±0.05	0.07±0.03	0.14±0.02	0.14±0.02	0.23±0.03	0.23±0.02	0.24±0.06
P	BDL	BDL	BDL	BDL	BDL	BDL	BDL
Ti	BDL	BDL	BDL	BDL	BDL	BDL	BDL
Cr	0.02±0.00	0.01±0.00	0.01±0.00	0.01±0.00	BDL	0.01±0.00	0.01±0.00
Ni	1.04±0.02	0.78±0.01	0.72±0.01	0.70±0.02	0.71±0.01	0.58±0.01	0.55±0.01
Mn	BDL	8.2±0.8	45.9±0.5	61.8±1.7	96.4±1.0	141.6±1.3	164±10
Fe	620.0±0.3	595.7±0.3	553.7±0.8	536.9±2.0	544.3±1.2	440.7±1.2	416.1±0.6
Cu	BDL	BDL	BDL	BDL	BDL	0.01±00.0	BDL
Zn	0.05±0.01	BDL	BDL	BDL	BDL	BDL	BDL